Weak precipitation δ^2H response to large Holocene hydroclimate changes in eastern North America

Ioana C. Stefanescu[1*], Bryan N. Shuman[1], Laurie D. Grigg[2], Adriana Bailey[3], Vania Stefanova[4], W. Wyatt Oswald[5]

[1*]Department of Geology and Geophysics, University of Wyoming

[2]Department of Earth and Environmental Sciences, Norwich University

[3]National Center for Atmospheric Research, Boulder, Colorado

[4]Continental Scientific Drilling Facility and Limnological Research Center, University of Minnesota

[5] Marlboro Institute for Liberal Arts and Interdisciplinary Studies, Emerson College, Boston, MA

Corresponding author: Ioana C. Stefanescu

Address: 1000 E University Ave, Science Initiative Room 4234, Laramie, Wyoming, 82071, United States of America

E-mail: *istefane@uwyo.edu*

ABSTRACT

In eastern North America, annual precipitation increased by >40% over the Holocene, largely in response to melting of the Laurentide Ice Sheet. The change substantially raised lake levels and transformed conifer-dominated ecosystems into mesic deciduous forests. δ^2H values of terrestrially derived leaf-wax *n*-alkanes can facilitate diagnoses of the climate dynamics involved by reconstructing δ^2H values of mean annual precipitation (δ^2H_{MAP}). However, competing influences on δ^2H_{MAP} values in the mid-latitudes, such as changes in moisture sources and in the seasonal distribution of precipitation, can generate confounding effects. To test δ^2H_{MAP} sensitivity to potential changes associated with the final Holocene phases of deglaciation in eastern North America, we used 14 fossil-pollen records to reconstruct monthly precipitation changes and to model δ^2H_{MAP} values during the Holocene. The pollen-inferred precipitation increased by 100-200 mm during both cold and warm seasons, but modelled δ^2H_{MAP} values changed by only ~10‰, because isotopically-heavy summer precipitation increased by nearly as much as the cold-season isotopically-light winter precipitation. Three new leaf wax *n*-C_{29}-alkane (δ^2H_{C29}) records spanning the Holocene from Vermont, Pennsylvania, and Massachusetts closely follow modeled δ^2H_{MAP} trends and confirm only a small decline in δ^2H_{MAP} values over the Holocene. Because the shifts in precipitation seasonality accurately predict the *n*-alkane records, changes in moisture sources or pathways appear to play only a minor role in the regional δ^2H_{MAP} history despite the effects of deglaciation on atmospheric circulation. Soil evaporation also did not significantly alter δ^2H_{C29} values from the values predicted using the pollen-derived reconstructions. The results affirm that δ^2H_{C29} values faithfully detected anticipated isotopic changes in δ^2H_{MAP} values, but that important paleoclimate events may not always yield strong changes in δ^2H_{MAP} values.

1. INTRODUCTION

Due to the geographic position of the northeastern United States, the region has experienced major climate changes over the Holocene (~11.7 kyrs to present) driven by the retreat of the Laurentide Ice Sheet (LIS), orbitally-forced insolation changes, and the dynamics of the adjacent North Atlantic Ocean (Webb et al., 1993; Shuman and Marsicek 2016; Shuman and Plank, 2011; Shuman et al., 2019). An early Holocene (~8 ka) shift from ice-sheet-dominated climate trends to those driven by seasonal insolation changes triggered a >40% increase in regional precipitation and a major shift from conifer to deciduous forests (Shuman et al., 2002; Shuman et al., 2009; Oswald et al., 2018; Shuman et al., 2019). The accelerated decline of the LIS around ca. 8.2 ka likely had implications for regional atmospheric circulation, the frequency of different types of precipitation events (e.g., 'nor'easter' storms, tropical cyclones), and the seasonality of precipitation, while summer insolation anomalies likely influenced evaporation rates (Shuman and Donnelly, 2006). Stable isotope records may provide insight into how such processes contributed to the large hydroclimate and ecosystem changes (e.g., Kirby et al., 2002; Gao et al., 2017; Hou et al., 2007; Shuman et al., 2006; Mandl et al. 2016). However, amid these large Holocene climate shifts, *n*-C_{29} δ^2H records (δ^2H_{C29}) from the northeastern U.S., such as from the Adirondack Mountains (New York), suggest a limited range of variation in the δ^2H composition of precipitation over the Holocene (~10‰; Schartman et al., 2020). This pattern extends further west into Wisconsin where the δ^2H record from Lake Geneva also shows little variability over the Holocene (Puleo et al., 2020).

The δ^2H_{C29} records pose a fascinating paradox because a lack of δ^2H change during large-scale regional transformation defies expectations about both the climate changes involved and the sensitivity of δ^2H_{C29} records to mid-latitude hydroclimatology. Here, we explore the conundrum. In doing so, we use a multi-proxy context and the dynamic hydroclimate history of the northeastern U.S. as an opportunity to evaluate how networks of δ^2H_{C29} records represent hydrologic changes in the mid-latitudes.

Leaf wax *n*-alkanes preserved in sedimentary archives are increasingly being used here and elsewhere to reconstruct past moisture trends (Schefuß et al., 2005; Tierney et al., 2010; Rach et al., 2014; Basu et al., 2019; Cao et al., 2020; Puleo et al., 2020; Schartman et al., 2020; Toney et al., 2020). *n*-Alkanes are odd-numbered hydrocarbons synthesized by both terrestrial and aquatic plants using environmental waters that ultimately originate from precipitation (Sachse et al., 2012). Therefore, δ^2H_{wax} reflects the δ^2H composition of precipitation. Strong relationships at both regional and global scales between the δ^2H values of mean annual precipitation (δ^2H_{MAP}) and those of terrestrial plants leaf-waxes (i.e., *n*-C_{29}-alkane) make these compounds a suitable proxy for inferring the δ^2H values of past precipitation (Sachse et al., 2004; Sachse et al., 2006; Garcin et al., 2012; Sachse et al., 2012; Tipple et al., 2013; Freimuth et al., 2017; McFarlin et al., 2019; Stefanescu et al., in press). As the δ^2H values of precipitation at a given location are strongly controlled by atmospheric circulation and rainout processes (Craig 1961; Gat 1996; Dansgaard 1964), the δ^2H values of terrestrial leaf-waxes provide an opportunity to reconstruct the drivers behind past climate changes such as shifts in atmospheric circulation and moisture sources.

Here, we expand the leaf wax *n*-C_{29} δ^2H datasets from the northeastern U.S. region to include new coastal, inland, and northern records and compare the *n*-C_{29}-alkane-based reconstructed δ^2H values of mean annual precipitation ($\delta^2H_{MAP\_C29}$) to pollen-inferred expectations of precipitation δ^2H change (δ^2H_{MAP}). We first confirm that fossil pollen records from across the region indicate major changes in moisture availability, consistent with previous analyses of regional pollen data (Webb et al., 1993; Marsicek et al., 2013; Shuman et al., 2019) and lake-level reconstructions (Shuman et al., 2001; Newby et al., 2011; 2014; Shuman et al., 2019). Then, to understand potential outcomes in the $\delta^2H_{MAP\_C29}$ records, we combine the pollen-inferred precipitation history with modern values of δ^2H in monthly precipitation to test the sensitivity of δ^2H_{MAP} to the observed changes in precipitation seasonality alone (i.e., without accounting for changes in sources, circulation, and other influences on monthly δ^2H values). Finally, we compare the simulated δ^2H_{MAP} expectations with the three new $\delta^2H_{MAP\_C29}$ records from Vermont, Pennsylvania, and Massachusetts and assess both the temporal trends and spatial isotopic patterns to evaluate the roles of three major factors: (1) changes in precipitation seasonality, (2) changes in moisture sources and pathways, and (3) evaporative effects on soil moisture. The results have implications for interpreting the sensitivity of $\delta^2H_{MAP\_C29}$ to complex, multi-dimensional hydroclimate changes and can help establish benchmark expectations for isotope-enabled climate model simulations of the early Holocene (i.e., a strong regional precipitation change associated with a modest δ^2H_{MAP} change).

2. MATERIALS AND METHODS

2.1. Study sites

We present three new leaf-wax *n*-C_{29}-alkane records from Twin Ponds (Vermont), Blanding Lake (Pennsylvania) and Crooked Pond (Massachusetts) (Figure 1, Table 1). Twin Ponds fills two adjoining glacially-scoured basins within the limestone member of the Waits River Formation in east-central Vermont and is surrounded by northern hardwood forest dominated by a mix of angiosperm and gymnosperm tree species such as sugar maples (*Acer saccharum*), American beech (*Fagus grandifolia*), and eastern hemlock (*Tsuga canadensis*) (Grigg et al., 2021). Crooked Pond is a small kettle lake composed of two basins within sandy outwash near coastal Massachusetts. Pines (*Pinus* spp.) and oak (*Quercus* spp.) dominate the surrounding sand-plain vegetation (Shuman et al., 2001). The sandy soils limited vegetation changes at Crooked Pond during the Holocene (Shuman et al., 2001). We use the near-by pollen record from Deep-Taunton Pond (Oswald et al., 2018), located on adjacent glacial tills and surrounded by oak-dominated deciduous forest, to represent the regional vegetation changes near Crooked Pond. Blanding Lake occupies a basin in glacial till in a valley incised within the Allegany Plateau in northeastern Pennsylvania and is underlain by fluvial sandstones of the Catskill Formation. The immediate watershed contains a plantation of white pine (*Pinus strobus*) and mixed deciduous forest dominated by oak species (*Quercus* spp.) (Shuman and Burrell, 2017).

Sediment cores from Twin Ponds, Blanding Lake and Crooked Pond were collected using a hand-driven piston corer with 70 mm polycarbonate tubes. The total sediment core lengths were 4.83 m, 10.12 m and 6.13 m, respectively. The Twin Ponds sediment core was collected at a shallow water depth of 0.79 m, in a carbonate bench adjacent to the shore, while the sediment cores from Blanding Lake and Crooked Pond were collected from the deepest locations within the lakes at water depths of 5.55 m and 4.25 m, respectively. An additional core was also collected from 7.8 m of water at the center of Twin Ponds western basin. Age models for the 0.79 m depth sediment core from Twin Ponds, and for the sediment cores from Blanding Lake and Crooked Pond were derived from radiocarbon dates (Figure 2, Table 2) calibrated to calendar years using the bchron package with the IntCal20 calibration curve (Haslett and Parnell, 2008; Reimer et al., 2020). We also generated new chronologies for the $\delta^2H_{MAP\_C29}$ records at Heart and Moose lakes (Schartman et al., 2020) using IntCal20.

2.2. n-Alkane extraction and instrumental analysis

n-Alkanes were extracted from 2-8 grams freeze-dried sediment and analyzed for δ^2H on a Thermo Scientific Trace GC coupled to a Thermo Delta V IRMS following the methods of Stefanescu et al. (in press). All samples were run in duplicates. A standard *n*-alkane mixture (mixture A7 from Arndt Schimmelmann, Indiana University) containing alkanes *n*-C_{16} to *n*-C_{30} was used to identify *n*-alkane compounds based on retention times, and to account for instrument D/H offset. The average H_3^+ factor for all runs was 2.19 and ranged between 1.98 to 2.21 across all runs. All δ^2H measurements are reported in ‰ relative to the Vienna Standard Ocean Water (VSMOW). Sample duplicate δ^2H measurements were averaged, and the average standard deviation of duplicates was 2.4 ‰ across all runs.

The δ^2H_{C29} analysis at Twin Ponds was completed on the shallow carbonate core where additional oxygen isotope analyses will also be possible for future comparison. To compare the range of δ^2H_{C29} values between the two cores, we also analyzed δ^2H_{C29} values in four sediment samples from the sediment core collected at a water depth of 7.8 m. From here on, we refer to the sediment core collected near the shore at the water depth of 0.79 m as the "shallow water core" and to the core collected from the lake center and a depth of 7.8 m as the "deep water core".

We use *n*-C_{29}-alkane δ^2H values to infer δ^2H_{MAP} values by applying the North American average apparent fractionation factor (ε_{app}) of -131‰ (Stefanescu et al., in press). The inferred Holocene $\delta^2H_{MAP\_C29}$ values at each lake were calculated as follows:

$$\delta^2H_{MAP\_C29}‰ = 1000 \text{ x } \left[\frac{\delta^2H_{C29}‰ + 1000}{-131‰ + 1000} - 1\right] \quad \text{Eq.1}$$

2.3. Pollen analysis and climate reconstructions

We present new fossil pollen records from Twin Ponds (VT) and Blanding Lake (PA) (Figure 1, Table 1) as part of an effort to compare the inferred $\delta^2H_{MAP\_C29}$ values to pollen-inferred estimates of Holocene hydroclimate changes and their isotopic consequences. Sediment samples from Twin Ponds (VT) and Blanding Lake (PA) were prepared for pollen analysis following a standard procedure (Faegri and Iversen. 1975) and analyzed for fossil pollen and spores. Pollen of aquatic plants, fern, mosses, and fungal spores were excluded from the pollen sum. The results are presented as percentages, calculated relative to the sum of all terrestrial taxa and simplified pollen diagrams for the two lakes include the major pollen types discussed in the text (Figure 4). For regional comparison, an additional 12 fossil-pollen records were obtained from the Neotoma Palaeoecological Database (Figure 1, Table 1) (Williams et al., 2018). This network of detailed pollen records was used to examine the coherency between local and regional pollen-based moisture reconstructions over the Holocene. We use detailed fossil pollen records from 14 sites in the region (Figure 1, Table 1) including Twin Ponds (VT), Blanding Lake (PA), and Heart Lake (NY) (Whitehead and Jackson, 1990). Chronologies for all pollen records were updated using the bchron package with the IntCal20 calibration curve (Parnell et al., 2008; Reimer et al., 2020).

We reconstructed monthly precipitation changes from the pollen data at the 14 sites (Figure 1, Figure 5, Figure 6) using the modern analogue technique, which compares each fossil pollen sample to their most analogous modern pollen samples (Overpeck et al., 1985). The modern monthly precipitation rates associated with the modern pollen samples are assumed to represent the paleoclimate conditions as has been done previously for this region (e.g., Marsicek et al., 2013). The modern pollen samples were derived from sites in North America east of 95°W and were compared to the fossil pollen samples using the squared-chord distance (SCD) metric (Overpeck et al., 1985). The comparisons measure the differences in the relative abundances of 54 important regional pollen types (Marsicek et al., 2013). The five modern pollen samples with the lowest SCDs were considered analogs for each fossil pollen sample. The modern mean monthly precipitation from the location of each analog was obtained from Whitmore et al. (2005) and then the values for the five analogs were averaged and assigned as the paleo-precipitation values. While the approach is imperfect, it builds upon the ability of the modern analog technique to reconstruct precipitation during all seasons (Williams and Shuman, 2008). Warm and cold season precipitation totals (Figure 6) were calculated by summing the reconstructed monthly precipitation for June-November and December-May, respectively, while the warm/cold season precipitation ratio was calculated by dividing their sums.

2.4. Modern and modeled δ^2H values of precipitation

Modern monthly and mean annual precipitation (MAP) δ^2H values were obtained using the Online Isotopes of Precipitation Calculator (OIPC) (Bowen, G. J., 2020) and are reported relative to VSMOW (Figure 1, Figure 3A). Modern monthly and mean annual precipitation inputs (mm) were obtained from the Parameter-Elevation Regressions on Independent Slopes Model (PRISM) with a resolution of 800 m, from the Climate Group at Oregon State University (Prism Climate Group, 2021; Figure 3B, Table 1). To test the accuracy of OIPC δ^2H values, we compare OIPC monthly and annual δ^2H values to measured monthly precipitation and soil moisture δ^2H values from the nearby site of Hubbard Brook, New Hampshire (Figure 1A,B; Campbell and Greene, 2019).

As pollen-inferred precipitation changes suggest that modern precipitation in the region generally exceeds the rates of the last 14 kyrs (Webb et al., 1993; Shuman et al., 2019), we model the potential sensitivity of δ^2H_{MAP} to reduced seasonal precipitation rates. To do so, we first computed percent decreases from modern precipitation values (in 10 % increments) for warm-season (June-November) and cold-season (December-May) precipitation, respectively, which we combined with modern monthly δ^2H values to calculate expected δ^2H_{MAP} values as in Eq.2. The results estimate how the reduction in precipitation in either season today would alter the total isotopic composition of annual precipitation (δ^2H_{MAP}) by shifting the weighting of isotopic inputs in favor of the other season:

$$\text{Modeled } \delta^2H_{MAP}‰ = \frac{\sum(P_{month}(mm) \times \delta^2H_{month}(‰))}{MAP\ (mm)} \qquad \text{Eq.2}$$

where P_{month} represents the mean precipitation amount of each month from January to December and where δ^2H_{month} equals a fixed value for each month at each site as determined by OIPC.

We then compute expected δ^2H_{MAP} departures from modern OIPC δ^2H_{MAP} values using Eq. 3:

$$\Delta\delta^2H_{MAP}‰ = \text{modern } \delta^2H_{MAP}‰ - \text{modeled } \delta^2H_{MAP}‰ \qquad \text{Eq.3}$$

To examine the effect of the inferred changes in precipitation seasonality over the past 14 kyrs, we then repeated this modelling of δ^2H_{MAP} using Eq. 2 by combining the monthly precipitation input (mm) reconstructed from the fossil pollen with the fixed modern monthly precipitation δ^2H values from OIPC at each pollen site. The goal is to estimate the sensitivity of δ^2H_{MAP} values to the reconstructed seasonal precipitation changes alone and then compare with the measured $\delta^2H_{MAP\_C29}$ values to diagnose attendant changes in vapor sources, circulation pathways, precipitation mechanisms, or soil evaporation, which we assume would create departures from modeled δ^2H_{MAP} values in the measured $\delta^2H_{MAP\_C29}$ values.

3. RESULTS AND DISCUSSION

3.1. Modern precipitation δ^2H values in the northeastern U.S. and their sensitivity to change

Modern monthly precipitation and soil water δ^2H values measured at Hubbard Brook (Figure 1B; Campbell and Greene, 2019) show 40‰-60‰ seasonal variation and a 3‰ difference in δ^2H_{MAP} values, suggesting little evaporation effects on soil water δ^2H values. These findings indicate that terrestrial leaf wax source water (i.e., soil moisture) should closely track the δ^2H composition of MAP with minimal evaporation effects. Moreover, modeled monthly and annual δ^2H values at Hubbard Brook (NH) parallel those of measured precipitation and are similar to those modeled at Twin Ponds, VT (Figure 1B). Furthermore, modeled δ^2H values match those observed at Hubbard Brook suggesting that OIPC (Bowen, 2020) is suitable for predicting modern monthly and annual δ^2H values across the region.

Modern monthly precipitation δ^2H values (from OIPC) range from -132 to -11‰ across the region (Figure 3A) with the most negative values observed at the inland sites from New York, Vermont and Pennsylvania where the range in monthly δ^2H values is -132 to -21‰. A smaller range in monthly δ^2H values of -90 to -11‰ is observed at the coastal sites of Massachusetts. Modern monthly precipitation values (from PRISM) range from 50 to 140 mm across the region (Figure 3B) and show distinctive seasonality patterns. The inland sites receive more precipitation during the warm season while the coastal sites of Massachusetts receive more even monthly precipitation totals with modest peaks during March-April and November-December (purple shading, Figure 3B).

Estimating the change in δ^2H_{MAP} values using Eq. 2 and 3 reveals that a decrease in either cold- or warm-season precipitation inputs would only have a moderate effect on δ^2H_{MAP} values across the region (Figure 3C,D). For example, a 50% reduction in cold-season precipitation would only increase δ^2H_{MAP} values by a maximum 10.6‰. Conversely, a 100% reduction would only lead to a maximum increase of 23.4‰. Similarly, 50% and 100% reductions in warm-season precipitation would only decrease δ^2H_{MAP} values by up to 8.1‰ and 27.6‰, respectively. Furthermore, combined reductions in both cold- and warm-season precipitation inputs would likely neutralize changes in δ^2H_{MAP} values across the region as an increase of ~10‰ driven by halving winter precipitation could be offset by a decrease of ~8‰ resulting from a halving of summer precipitation, yielding a net effect of only ~2‰.

Additionally, our model shows that decreases in cold- or warm-season precipitation would produce greater changes in δ^2H_{MAP} values at the inland sites compared to the coastal sites of Massachusetts (Figure 3C). For example, because cold-season precipitation δ^2H values at the inland sites (mean of -91‰) are lower than at the coastal sites (mean of -63‰), a decrease in cold-season precipitation would generate larger changes in δ^2H_{MAP} values at the inland sites.

3.2. Pollen-inferred vegetation changes

Pollen-inferred vegetation changes at Heart Lake (NY), Twin Ponds (VT), Blanding Lake (PA), and Deep-Taunton Pond (MA) all include a significant transition at 9-8 kyrs BP from abundant conifer tree species, such as *Picea* and *Pinus* (green shading, Figure 4) to broadleaved deciduous species, such as *Quercus* (maroon shading, Figure 4). During the past 8 kyrs, *Quercus* pollen was most abundant in southeastern Massachusetts at Deep-Taunton Pond as well as at Crooked Pond (Shuman et al., 2001), but *Betula* and *Fagus* pollen became important at the three mixed forest sites, Heart Lake, Twin Ponds, and Blanding Lake (Figure 4). At these sites, *Tsuga* also remained an important conifer after 8 kyr B.P. (light green, Figure 4), but all four pollen records capture a sharp decline in *Tsuga* abundance from ca. 5.5-3 kyrs B.P. when deciduous angiosperms became most abundant across the region. Afterwards, some conifer taxa, such *Tsuga* and *Pinus*, increased in abundance but never recovered the dominance observed before 8 kyrs B.P. Grass (Poaceae) pollen remained low throughout the records indicating the dominance of forests until the historic land clearance of the past 300 yrs.

Regionally, the dominant conifers of late Pleistocene and early Holocene vegetation suggest a cold and dry climate during the early Holocene (Webb et al., 1993). The major shift in vegetation from conifer forests to deciduous forests by 8 ka is consistent with a change towards a warm and wet climate during most of the Holocene after the collapse of LIS (Shuman et al., 2002). Consistent with lake-level reconstructions from the region (Shuman and Burrell, 2017), the increased abundance of mesic (highly moisture-dependent) taxa, such as *Betula*, *Fagus*, and *Tsuga* indicate an increase in regional moisture availability after 9-8 kyrs B.P. (Webb et al., 1993; Marsicek et al., 2013; Shuman et al., 2019),

3.3. Pollen-inferred precipitation seasonality

Changes in precipitation inputs reconstructed using the modern analog technique show sub-regional coherency and major seasonality changes over the past 14 kyrs (Figure 5). Late Pleistocene and early Holocene precipitation inputs were lower than today (yellow lines are lower than purple lines in Figure 5), while late Pleistocene and early Holocene (yellow lines, Figure 5) precipitation inputs are characterized by greater precipitation seasonality compared to modern (dark purple, Figure 5). Furthermore, the increase in Holocene precipitation inputs was smaller during the summer months than during the winter months. Early Holocene precipitation regimes across the entire region appear to have been dominated by summer precipitation inputs, similar to the modern precipitation inputs observed in the inland areas of New York and Vermont today (Figure 5).

In contrast, the mid- to late Holocene is characterized by low precipitation seasonality as winter months precipitation inputs increased substantially during the Holocene (Figure 5). Eastern and coastal areas in Pennsylvania and Massachusetts have undergone the largest changes in precipitation seasonality over the past 14 kyrs. Both regions show increases of >70 mm during winter months and an increase of <40 mm during summer months. In comparison, the sites in New York and Vermont show an increase in winter precipitation of ~50 mm/month and an increase in summer precipitation of ~35 mm/month (Figure 5).

3.4. Pollen-inferred hydroclimate trends

Time series of pollen-inferred seasonal precipitation changes reveal several important details on the time evolution of regional hydroclimate (Figure 6A). The reconstructions show three distinctive hydroclimate features: (1) a wet Younger-Dryas interval (12.9-11.7 ka), more prominent at the northern sites (NY and VT) than at the southern or coastal sites (PA and MA), which is consistent with other lines of evidence for increased precipitation during this time interval in the region (Grigg et al., 2021); (2) a region-wide dry early Holocene (11.7-8.2 ka); and (3) a progressive increase in precipitation during the mid- to late Holocene (>6 ka-present) particularly in Massachusetts near the North Atlantic coast and not in Vermont. The entire region has seen a reduction in the warm/cold season ratio of precipitation such that seasonal precipitation inputs are close to being equal during the late Holocene. In contrast, early Holocene warm season precipitation inputs were twice those of the cold season (Figure 6B).

These precipitation trends are attributable to ocean circulation changes during the Younger-Dryas interval and to the presence of the ice sheet until ca. 8 ka. Both factors could have altered advection of moisture into the region. During the Younger-Dryas interval, sea surface temperature changes over the North Atlantic may have temporarily altered the storm track along the east coast of North America, delivering increased moisture in the region (Kirby et al., 2002). Equally, the persistence of a glacial anti-cyclone over the ice sheet until ca. 8 ka would have limited the northward advection of moisture into the region (Shuman et al., 2002). The loss of the ice sheet is perhaps the single largest driver behind the rapid increase in precipitation inputs between early and mid-Holocene, while other factors such as insolation anomalies probably drove precipitation changes into the late Holocene (Shuman and Marsicek, 2016).

At the inland sites, both cold- and warm-season precipitation increase towards modern values after ~10 ka, but cold-season precipitation increased more than warm-season precipitation (Figure 7). Therefore, both seasons contribute nearly equally from 8 ka to present. At the coastal site of Deep-Taunton, cold-season precipitation inputs during the late Pleistocene were ~40% lower than modern. At this site, cold-season precipitation inputs after 8 ka increased further by another ~30%. In contrast, this coastal site saw little change in warm-season precipitation inputs during the past 14 kyrs (~15% of modern).

3.5. Modeled δ^2H_{MAP} values during the past 14kyrs

The potential impacts of the reconstructed changes in precipitation seasonality on δ^2H_{MAP} were tested using Eq.2. To predict the potential magnitude of δ^2H_{MAP} change related to the changing seasonality of precipitation over the past 14 kyrs. we combined modern monthly δ^2H values (OIPC) from individual pollen sites with pollen-inferred monthly precipitation inputs. The model assumes no change in monthly precipitation δ^2H values (i.e., it uses constant modern monthly OPIC δ^2H values), and shows that changes in seasonality alone would have caused δ^2H_{MAP} values to peak during the late Pleistocene (Figure 7B, orange lines). At the time, warm season precipitation inputs were ~20% higher than cold season precipitation inputs, which were at their lowest levels of the past 14 kyrs (40% of modern; Figure 7A). Although modeled δ^2H_{MAP} values decreased by ~10‰ across the region during the Holocene as cold season precipitation inputs increased, these modeled values were far more stable than the 10-40% change in seasonal precipitation (compare Figure 7A with orange lines in Figure 7B). These results agree with our modeled expectations of δ^2H_{MAP} values given seasonal changes in precipitation (Figure 3C,D).

Coastal sites like Deep-Taunton record larger increases in cold-season precipitation inputs (~60%) compared to the inland sites (Figure 6-7), but modeled and reconstructed cold-season δ^2H values are higher along the coast than at the inland sites (Figure 3A). Consequently, the high cold season δ^2H values at this site can offset an increase in cold season precipitation inputs creating a continuous decline in δ^2H_{MAP} values spanning over the last 14 kyrs (Figure 3C). These results are also consistent with the modest change in modeled δ^2H_{MAP} values inferred across the region (orange lines, Figure 7B).

3.6. Reconstructed $\delta^2H_{MAP\_C29}$ values during the past 14 kyrs

Reconstructed $\delta^2H_{MAP\_C29}$ values have similar magnitudes and directions of change across all sites (Figure 7B, blue lines). The reconstructed trends differ in detail, but except for Twin Ponds, the *n*-C_{29} records indicate that $\delta^2H_{MAP\_C29}$ values were ~10‰ more positive than today during early to mid-Holocene (Figure 7). Additionally, $\delta^2H_{MAP\_C29}$ values from New York and Vermont are typically ~20‰ lower than those from Pennsylvania and Massachusetts as expected from the modern isotopic gradients (e.g., as calculated by OPIC; Figure 3A). Although each record also contains unique patterns of high frequency variability of 20-40‰, the long-term trends generally conform with expectations simulated from the pollen data (compare orange and blue lines, Figure 7B).

As the model assumes no change in monthly precipitation δ^2H values over the past 14 kyrs, we hypothesize that the $\delta^2H_{MAP\_C29}$ trends would have deviated substantially from modeled δ^2H_{MAP} values if changes in moisture sources, pathways, or in soil evaporation regimes occurred in the past. The similarity between modeled and reconstructed δ^2H_{MAP} values suggests that the LIS presence limited the advection of subtropical moisture into the region and created extremely low annual precipitation inputs during the early Holocene. However, as proposed by Schartman et al. (2020), we find that moisture sources in the region remained the same. Moreover, if warm summers and high summer insolation during early and mid-Holocene affected soil water δ^2H values by enhancing evaporation, then the reconstructed $\delta^2H_{MAP\_C29}$ values would have been consistently more positive than the pollen-inferred δ^2H_{MAP} values. Yet the $\delta^2H_{MAP\_C29}$ records are either within or below the range of modeled δ^2H_{MAP} values, which indicates that soil evaporation did not play a major role in modifying soil moisture δ^2H values.

Consequently, our results show that the region's hydroclimate was likely modulated by the LIS presence and associated high-pressure, anticyclone atmospheric movements during the early Holocene (Shuman et al., 2002). However, after the final LIS collapse, the change in the frequency of northward advection of moisture especially during the winter did not substantially alter moisture sources and pathways (Figure 5 and 6). Furthermore, unless early Holocene soil evaporation closely offset a negative shift in δ^2H values driven by changes in atmospheric circulation, our $\delta^2H_{MAP\_C29}$ records and pollen-derived sensitivity test indicate that neither process dramatically changed δ^2H_{MAP} values despite the large climate forcing involved. With the final LIS collapse by ~8 ka, the region experienced major increases in seasonal precipitation inputs, but the relative balance of changes across seasons produced only small changes in δ^2H_{MAP} values (Figures 5-7). Therefore, these results confirm that $\delta^2H_{MAP\_C29}$ is sensitive to and tracks major changes in δ^2H_{MAP}, but the combined effects of seasonal changes in precipitation can reduce the amplitude of δ^2H_{MAP} signals compared to the associated seasonal precipitation changes (Figure 7). Interpretation of leaf-wax δ^2H records, therefore, can benefit from comparison with other hydroclimate reconstructions.

In addition to the major trends, the pollen-inferred precipitation regimes suggest century-scale variability across the region (Figs. 6 and 7), which is closely replicated by evidence for lake-level changes from the northeastern U.S. (Shuman et al., 2019). However, when monthly precipitation reconstructions were converted to δ^2H_{MAP} values using Eq. 2 (orange lines, Figure 7B), the century-scale variability – and longer events such as the anomalously high precipitation during the Younger Dryas – were not detected. The lack of century-scale variability in modeled δ^2H_{MAP} values arises, in isotope space, for the same reason that the long-term trends experienced only small changes in δ^2H_{MAP} values: even large percentage changes in total precipitation produce small net changes in δ^2H_{MAP} values (Figure 3). This is especially the case when the same direction of precipitation change occurs in different seasons, yielding opposite isotopic direction of changes that cancel each other. Moreover, the $\delta^2H_{MAP\_C29}$ records indicate large centennial-scale isotopic variability, but this variability is neither consistent with the patterns expected from the pollen nor consistent across sites (Figure 7B). This centennial isotopic variability could represent shifts in precipitation sources as the reconstructed values exceed the calibration uncertainty (1 s.d.=12‰; Stefanescu et al., in press). However, the low temporal resolution of our *n*-C_{29} records prevents us from making inferences about centennial scale shifts in precipitation sources. Twin Ponds (VT) may highlight one of the most extreme examples of other potential influences.

3.7. $\delta^2H_{MAP\_C29}$ anomaly at Twin Ponds, Vermont

The Twin Ponds $\delta^2H_{MAP\_C29}$ record shows a substantial deviation from modeled δ^2H_{MAP} values and regional $\delta^2H_{MAP\_C29}$ patterns (Figure 7B). However, the two New York $\delta^2H_{MAP\_C29}$ records (Figure 7B, Schartman et al., 2020) do not show the same anomaly and are inconsistent with a regional change in circulation pathways or sources across the northern part of the region. Due to the geographic proximity and climate similarity of Twin Ponds and the two New York sites, we infer that this particular sediment record was likely influenced by lake specific variations, such as changes in *n*-C_{29}-alkane source.

Pollen-inferred vegetation changes at and near our sites (Figure 4) show a shift from a gymnosperm- to an angiosperm-dominated vegetation during the Holocene. Average fractionation factors between *n*-C_{29}-alkane and precipitation δ^2H values are comparable for gymnosperms and angiosperms (within 6‰; Stefanescu et al., in press). Moreover, the vegetation shift is not unique to Twin Ponds (Figure 4). Therefore, the early Holocene vegetation transition is an unlikely explanation for the prolonged negative anomaly in $\delta^2H_{MAP\_C29}$ values at Twin Ponds.

Even though *n*-C_{29}-alkane is predominantly synthesized by terrestrial plants, aquatic plants can also synthesize *n*-C_{29}-alkane in small amounts and could be an additional source of unusual isotopic values. An aquatic source may be particularly important at Twin Ponds where our primary core was collected from a productive littoral bench distal from the inlet, at a shallow depth of only 0.79 m. The fractionation factor between the aquatically produced *n*-C_{29}-alkane and δ^2H_{MAP} (ε_{app}) is ~30‰ larger than that of terrestrial plants (Stefanescu et al., in press), therefore, a shift to aquatically produced *n*-alkanes would generate a negative excursion in reconstructed $\delta^2H_{MAP\_C29}$ values at Twin Ponds. Littoral terrestrial vegetation such as grasses may also be an important additional source. ε_{app} in grasses is also ~30‰ larger than in terrestrial plants (Stefanescu et al., in press) and, therefore, *n*-C_{29} compounds derived from grasses would also generate a negative excursion in reconstructed $\delta^2H_{MAP\_C29}$ values.

To evaluate the potential role of alternative *n*-C_{29}-alkane sources within the lake, we measured *n*-C_{29} δ^2H values in four sediment samples derived from the deep-water core collected at a depth of 7.8 m from Twin Ponds (Figure 7B; black squares). δ^2H values for these four samples spanning over the mid-Holocene differ significantly from the $\delta^2H_{MAP\_C29}$ trends observed in the shallow core (blue line, Figure 7B). Furthermore, the reconstructed $\delta^2H_{MAP\_C29}$ values fall within the range of modeled δ^2H_{MAP} based on the pollen data (orange lines, Figure 7B). Despite the small number of samples derived from the deep-water core, the data shows major differences in $\delta^2H_{MAP\_C29}$ values between the shallow and deep-water cores, as well as in the long-term $\delta^2H_{MAP\_C29}$ trends. Given that proximity to shore can drive a dominant aquatic and grass input of *n*-C_{29}-alkane into lake sediments, and that both aquatic plants and grasses have higher ε_{app} values compared to those of higher terrestrial plants, we infer that the negative excursion in reconstructed $\delta^2H_{MAP\_C29}$ values in the shallow-water core at Twin Ponds was driven by increased aquatic or grass inputs. Further analysis is needed to quantify *n*-C_{29}-alkane sources and their δ^2H values in the deep-water core in order to assess the amount of aquatic and grass input and its effects on *n*-C_{29} δ^2H values within lakes.

4. CONCLUSIONS

Our new leaf-wax δ^2H records from the northeastern U.S. suggest a small change in δ^2H_{MAP} values over the past 14 kyrs. The new *n*-alkane data agree with other, previously published records (Puleo et al., 2020; Schartman et al., 2020) and indicate little change in mean annual precipitation δ^2H values (δ^2H_{MAP}) during a major regional climate transition. The lack of major changes in δ^2H_{MAP} values poses a fascinating paradox, which we resolve by combining the modern distribution of monthly δ^2H values with the pollen-inferred changes in seasonal precipitation inputs to model the expected changes in δ^2H_{MAP} values given seasonality changes in precipitation inputs over the past 14 kyrs. Our model generates Holocene δ^2H_{MAP} expectations given only the reconstructed shifts in the seasonality of precipitation and does not account for changes in moisture sources, moisture pathways, or soil moisture evaporation, which may have influenced $\delta^2H_{MAP\_C29}$. The resulting agreement in the predicted δ^2H_{MAP} patterns and those measured with our new $\delta^2H_{MAP\_C29}$ records confirm that, although precipitation increased across the region, δ^2H_{MAP} decreased by only 10‰ due to a shift in the seasonality of precipitation.

We hypothesize that the LIS presence and associated anti-cyclone during the late Pleistocene and early Holocene likely prevented the advection of moisture into the region especially during the winter. The pattern explains the low precipitation rates inferred from the pollen data, except when unusual conditions over the North Atlantic favored high precipitation during the Younger Dryas. However, neither change produced large variations in the isotopic values of regional precipitation. Subsequently, the LIS collapse by 8 ka allowed cold-season precipitation to increase such that both cold- and warm-season precipitation fell more equally across the region since 8 ka. However, these seasonal changes in precipitation, which affected both the vegetation and regional lake levels, translated to only minor changes in δ^2H_{MAP} values. These results suggest that precipitation inputs in the region were not modulated by changes in moisture sources or moisture pathways over the past 14 kyrs. Consequently, our results show that $\delta^2H_{MAP\_C29}$ records are sensitive to δ^2H_{MAP} changes in the mid-latitudes, but changes in δ^2H_{MAP} values can be dampened by counterbalancing shifts in seasonal precipitation changes.

ACKNOWLEDGMENTS

We thank Chandelle Macdonald and Craig Cook for help with GC-IRMS analyses. This work was supported by the National Science Foundation Grant 1146297 and EPS-1655726. Adriana Bailey acknowledges support from the National Center for Atmospheric Research, which is a major facility sponsored by the National Science Foundation under Cooperative Agreement 1852977.

DATA AVALIABILITY

Data associated with this article can be found at https://doi.org/10.15786/20126495.

REFERENCES

Basu, S., Sanyal, P., Pillai, A.A. and Ambili, A., 2019. Response of grassland ecosystem to monsoonal precipitation variability during the Mid-Late Holocene: Inferences based on molecular isotopic records from Banni grassland, western India. *PloS one*, *14*(4), p.e0212743.

Bowen, G. J. 2020: Gridded maps of the isotopic composition of meteoric waters. http://www.waterisotopes.org

Cai, S., and Z. Yu. 2011. Response of a warm temperate peatland to Holocene climate change in northeastern Pennsylvania. Quaternary Research 75:531-540.

Campbell, J. and M. Green. 2019. Water isotope samples from Watershed 3 at Hubbard Brook Experimental Forest, 2006-2010 ver 1. Environmental Data Initiative. https://doi.org/10.6073/pasta/f5740876b68ec42b695c39d8ad790cee (Accessed 2021-06-22)

Cao, M., Sun, J., Liu, W., Hou, J., Tian, Q. and Sun, Z., 2020. Paleoclimatic fluctuations inferred from leaf wax n-alkane records in Central Tibet in the late Oligocene to early Miocene. *Palaeogeography, Palaeoclimatology, Palaeoecology*, *539*, p.109504.

Craig H. 1961. Isotopic variations in meteoric waters. Science 133:1702–3 Craig

Dansgaard, W., 1964. Stable isotopes in precipitation. Tellus, 16(4), pp.436-468.

Faegri, K. and Iversen, J. (1975) Textbook of Pollen Analysis. Munksgaard, Copenhagen.

Freimuth, E.J., Diefendorf, A.F., Lowell, T.V., 2017. Hydrogen isotopes of n-alkanes and n-alkanoic acids as tracers of precipitation in a temperate forest and im- plications for paleorecords. Geochim. Cosmochim. Acta 206, 166e183. https://doi.org/10.1016/j.gca.2017.02.027.

Gao, L., Huang, Y., Shuman, B., Oswald, W.W. and Foster, D., 2017. A high-resolution hydrogen isotope record of behenic acid for the past 16 kyr in the northeastern United States. Quaternary International, 449, pp.1-11.

Garcin, Y., Schwab, V.F., Gleixner, G., Kahmen, A., Todou, G., Séné, O., Onana, J.M., Achoundong, G. and Sachse, D., 2012. Hydrogen isotope ratios of lacustrine sedimentary n-alkanes as proxies of tropical African hydrology: insights from a calibration transect across Cameroon. Geochimica et Cosmochimica Acta, 79, pp.106-126.

Gat, J.R., 1996. Oxygen and hydrogen isotopes in the hydrologic cycle. Annual Review of Earth and Planetary Sciences, 24, pp.225-262.

Craig, H., 1961. Isotopic variations in meteoric waters. Science, 133(3465), pp.1702-1703.

Grigg, L.D., Engle, K.J., Smith, A.J., Shuman, B.N. and Mandl, M.B., 2021. A multi-proxy reconstruction of climate during the late-Pleistocene to early Holocene transition in the northeastern, USA. Quaternary Research, pp.1-17.

Haslett J, Parnell AC, 2008. "A simple monotone process with application to radiocarbon-dated depth chronologies." *Journal of the Royal Statistical Society: Series C (Applied Statistics)*, **57**(4), 399–418. https://rss.onlinelibrary.wiley.com/doi/full/10.1111/j.1467-9876.2008.00623.x.

Hou, J., Huang, Y., Oswald, W.W., Foster, D.R. and Shuman, B., 2007. Centennial-scale compound-specific hydrogen isotope record of Pleistocene–Holocene climate transition from southern New England. Geophysical Research Letters, 34(19).

Ibe, R.A. 1982. Quaternary palynology of five lacustrine deposits in the Catskill Mountain region of New York. Dissertation. New York University, New York, New York, USA.

Kirby, M.E., Mullins, H.T., Patterson, W.P. and Burnett, A.W., 2002. Late glacial–Holocene atmospheric circulation and precipitation in the northeast United States inferred from modern calibrated stable oxygen and carbon isotopes. Geological Society of America Bulletin, 114(10), pp.1326-1340.

Mandl, M.B., Shuman, B.N., Marsicek, J. and Grigg, L., 2016. Estimating the regional climate signal in a late Pleistocene and early Holocene lake-sediment δ18O record from Vermont, USA. Quaternary Research, 86(1), pp.67-78.

Marsicek, J.P., Shuman, B., Brewer, S., Foster, D.R. and Oswald, W.W., 2013. Moisture and temperature changes associated with the mid-Holocene Tsuga decline in the northeastern United States. Quaternary Science Reviews, 80, pp.129-142.

McFarlin, J.M., Axford, Y., Masterson, A.L. and Osburn, M.R., 2019. Calibration of modern sedimentary δ2H plant wax-water relationships in Greenland lakes. Quaternary Science Reviews, 225, p.105978.

Newby, P.E., Shuman, B.N., Donnelly, J.P. and MacDonald, D., 2011. Repeated century-scale droughts over the past 13,000 yr near the Hudson River watershed, USA. Quaternary Research, 75(3), pp.523-530.

Oswald, W.W., Foster, D.R., Shuman, B.N., Doughty, E.D., Faison, E.K., Hall, B.R., Hansen, B.C., Lindbladh, M., Marroquin, A. and Truebe, S.A., 2018. Subregional variability in the response of New England vegetation to postglacial climate change. Journal of biogeography, 45(10), pp.2375-2388.

Overpeck, J.T., Webb III, T. and Prentice, I.C., 1985. Quantitative interpretation of fossil pollen spectra: dissimilarity coefficients and the method of modern analogs. Quaternary Research, 23(1), pp.87-108.

Parnell, A.C., Haslett, J., Allen, J.R., Buck, C.E., Huntley, B., 2008. A flexible approach to assessing synchroneity of past events using Bayesian reconstructions of sedimentation history. Quaternary Science Reviews 27, 1872–1885.

PRISM Climate Group, Oregon State University, http://prism.oregonstate.edu, created June 2021

Puleo, P.J., Axford, Y., McFarlin, J.M., Curry, B.B., Barklage, M. and Osburn, M.R., 2020. Late glacial and Holocene paleoenvironments in the midcontinent United States, inferred from Geneva Lake leaf wax, ostracode valve, and bulk sediment chemistry. Quaternary Science Reviews, 241, p.106384.

Rach, O., Brauer, A., Wilkes, H. and Sachse, D., 2014. Delayed hydrological response to Greenland cooling at the onset of the Younger Dryas in western Europe. Nature Geoscience, 7(2), pp.109-112.

Reimer, P.J., Austin, W.E., Bard, E., Bayliss, A., Blackwell, P.G., Ramsey, C.B., Butzin, M., Cheng, H., Edwards, R.L., Friedrich, M. and Grootes, P.M., 2020. The IntCal20 Northern Hemisphere radiocarbon age calibration curve (0–55 cal kBP). *Radiocarbon*, *62*(4), pp.725-757.

Sachse, D., Radke, J. and Gleixner, G., 2004. Hydrogen isotope ratios of recent lacustrine sedimentary n-alkanes record modern climate variability. Geochimica et Cosmochimica Acta, 68(23), pp.4877-4889.

Sachse, D., Radke, J. and Gleixner, G., 2006. δD values of individual n-alkanes from terrestrial plants along a climatic gradient–Implications for the sedimentary biomarker record. Organic Geochemistry, 37(4), pp.469-483.

Sachse, D., Billault, I., Bowen, G.J., Chikaraishi, Y., Dawson, T.E., Feakins, S.J., Freeman, K.H., Magill, C.R., McInerney, F.A., van der Meer, M.T.J.J., Polissar, P., Robins, R.J., Sachs, J.P., Schmidt, H.-L., Sessions, A.L., White, J.W.C., West, J.B., Kahmen, A., 2012. Molecular paleohydrology: interpreting the hydrogen- isotopic composition of lipid biomarkers from photosynthesizing organisms. Annu. Rev. Earth Planet. Sci. 40, 221e249. https://doi.org/10.1146/annurev- earth-042711-105535.

Schartman, A.K., Diefendorf, A.F., Lowell, T.V., Freimuth, E.J., Stewart, A.K., Landis, J.D. and Bates, B.R., 2020. Stable source of Holocene spring precipitation recorded in leaf wax hydrogen-isotope ratios from two New York lakes. *Quaternary Science Reviews*, *240*, p.106357.

Schefuß, E., Schouten, S. and Schneider, R.R., 2005. Climatic controls on central African hydrology during the past 20,000 years. Nature, 437(7061), pp.1003-1006.

Shuman, B., Bravo, J., Kaye, J., Lynch, J.A., Newby, P. and Webb, T., 2001. Late Quaternary water-level variations and vegetation history at Crooked Pond, southeastern Massachusetts. Quaternary Research, 56(3), pp.401-410.

Shuman, B., Bartlein, P., Logar, N., Newby, P. and Webb III, T., 2002. Parallel climate and vegetation responses to the early Holocene collapse of the Laurentide Ice Sheet. Quaternary science reviews, 21(16-17), pp.1793-1805.

Shuman, B. and Donnelly, J.P., 2006. The influence of seasonal precipitation and temperature regimes on lake levels in the northeastern United States during the Holocene. Quaternary Research, 65(1), pp.44-56.

Shuman, B., Huang, Y., Newby, P. and Wang, Y., 2006. Compound-specific isotopic analyses track changes in seasonal precipitation regimes in the Northeastern United States at ca 8200 cal yr BP. Quaternary Science Reviews, 25(21-22), pp.2992-3002.

Shuman, B.N., Newby, P. and Donnelly, J.P., 2009. Abrupt climate change as an important agent of ecological change in the Northeast US throughout the past 15,000 years. Quaternary Science Reviews, 28(17-18), pp.1693-1709.

Shuman, B. and Plank, C., 2011. Orbital, ice sheet, and possible solar controls on Holocene moisture trends in the North Atlantic drainage basin. Geology, 39(2), pp.151-154.

Shuman, B.N. and Marsicek, J., 2016. The structure of Holocene climate change in mid-latitude North America. Quaternary Science Reviews, 141, pp.38-51.

Shuman, B.N. and Burrell, S.A., 2017. Centennial to millennial hydroclimatic fluctuations in the humid northeast United States during the Holocene. Quaternary Research, 88(3), pp.514-524.

Shuman, B.N., Marsicek, J., Oswald, W.W. and Foster, D.R., 2019. Predictable hydrological and ecological responses to Holocene North Atlantic variability. Proceedings of the National Academy of Sciences, 116(13), pp.5985-5990.

Stefanescu I.C., Macdonald C., Cook Craig., Williams D., Shuman B.N., (In press). Mid- and long-chain leaf waxes δ^2H signatures in modern plants and lake sediments from mid-latitude North America. Geochimica et Cosmochimica Acta.

Suter, S.M. 1985. Late-glacial and Holocene vegetation history in southeastern Massachusetts: a 14,000 year pollen record. Current Research in the Pleistocene. Current Research in the Pleistocene 2:87-89.

Tierney, J.E., Russell, J.M. and Huang, Y., 2010. A molecular perspective on Late Quaternary climate and vegetation change in the Lake Tanganyika basin, East Africa. *Quaternary Science Reviews*, *29*(5-6), pp.787-800.

Tipple, B.J., Berke, M.A., Doman, C.E., Khachaturyan, S., Ehleringer, J.R., 2013. Leaf- wax n-alkanes record the plant-water environment at leaf flush. Proc. Natl. Acad. Sci. 110, 2659e2664. https://doi.org/10.1073/pnas.1213875110.

Toney, J.L., García-Alix, A., Jiménez-Moreno, G., Anderson, R.S., Moossen, H. and Seki, O., 2020. New insights into Holocene hydrology and temperature from lipid biomarkers in western Mediterranean alpine wetlands. *Quaternary Science Reviews*, *240*, p.106395.

Webb, R.S., Anderson, K.H. and Webb III, T., 1993. Pollen response-surface estimates of late-Quaternary changes in the moisture balance of the northeastern United States. Quaternary Research, 40(2), pp.213-227.

White, J.M., R.W. Mathewes, and W.H. Mathews. 1985. Late Pleistocene chronology and environment of the "ice-free corridor" of northwestern Alberta. Quaternary Research 24:173-186.

Whitehead, D.R., and S.T. Jackson. 1990. The regional vegetational history of the High Peaks (Adirondack Mountains), New York. Bulletin No. 478, New York State Museum, Albany, New York, USA.

Whitmore, J., Gajewski, K., Sawada, M., Williams, J.W., Shuman, B., Bartlein, P.J., Minckley, T., Viau, A.E., Webb Iii, T., Shafer, S. and Anderson, P., 2005. Modern pollen data from North America and Greenland for multi-scale paleoenvironmental applications. *Quaternary Science Reviews*, *24*(16-17), pp.1828-1848.

Williams, J.W., Grimm, E.C., Blois, J.L., Charles, D.F., Davis, E.B., Goring, S.J., Graham, R.W., Smith, A.J., Anderson, M., Arroyo-Cabrales, J. and Ashworth, A.C., 2018. The Neotoma Paleoecology Database, a multiproxy, international, community-curated data resource. *Quaternary Research*, *89*(1), pp.156-177.

Williams, J.W. and Shuman, B., 2008. Obtaining accurate and precise environmental reconstructions from the modern analog technique and North American surface pollen dataset. *Quaternary Science Reviews*, *27*(7-8), pp.669-687.

Table 1. Site locations and modern environmental parameters.

Site	Analysis	Latitude	Longitude	Elevation m	MAP mm	MAP δ^2H‰	MAAT °C	Citation
Brandreth Bog (NY)	pollen	43.92	-74.68	582	1193	-74	4.9.0	Overpeck, J.T. 1985
Heart Lake (NY)	pollen n-C_{29}	44.18	-73.97	665	1137	-76	5.0	Whitehead and Jackson 1990 Schartman et al., 2020
Moose Lake (NY)	n-C_{29}	44.37	-74.06	475	1075	-74	5.1	Schartman et al., 2020
Balsam Lake (NY)	pollen	42.03	-74.60	880	1381	-64	5.0	Ibe, R.A. 1982
Knob Hill (VT)	pollen	44.36	-72.37	378	1015	-70	5.7	Oswald et al., 2018
Twin Ponds (VT)	pollen n-C_{29}	44.06	-72.58	409	1072	-69	5.5	This study
Blanding Pond (PA)	pollen n-C_{29}	41.80	-75.68	454	1127	-59	7.6	This study
Spring Lake (PA)	pollen	41.67	-76.35	364	960	-60	8.2	White et al., 1985
Hubbard Brook (NH)	precipitation soil	43.78	-71.73	755	1129	-71	6.6	Campbell and Green, 2019
Black Pond (MA)	pollen	41.33	-70.79	13	1213	-43	10.4	Oswald et al., 2018
Crooked Pond (MA)	n-C_{29}	41.89	-70.65	45	1274	-46	9.9	This study
Deep- Falmouth Pond (MA)	pollen	41.56	-70.64	27	1260	-48	10.4	Oswald et al., 2018
Deep- Taunton Pond (MA)	pollen	41.88	-71.01	8	1260	-47	10	Oswald et al., 2018
Tannersville Bog (PA)	pollen	41.04	-75.26	282	1307	-51	9.2	Cai and Yu, 2011
Uncle Seth's Pond (MA)	pollen	41.43	-70.66	20	1251	-43	10.4	Oswald et al., 2018
Upper Wallface Pond (NY)	pollen	44.15	-74.06	981	1413	-80	3.7	Whitehead and Jackson, 1990
Winneconnet Pond	pollen	41.97	-71.12	22	1265	-48	10.0	Suter, S.M. 1985.

Table 2. Radiocarbon analyses.

Lake	Depth (m)	Thickness (cm)	Lab No.	Material	^{14}C yr B.P.	Error (yr)	Calibrated age range B.P. 5%	Median	95%
Twin Ponds	42	2	UCIAMS-127563	Charcoal	1530	15	1365	1391	1454
Twin Ponds	76.5*	1	UCIAMS-127562	Charcoal	430	15	482	499	509
Twin Ponds	162.5	1	UCIAMS-127561	Charcoal	3040	25	3177	3248	3332
Twin Ponds	266.5	1	UCIAMS-127560	Charcoal	4225	25	4659	4758	4841
Twin Ponds	386.5**	2	UCIAMS-121904	core 48	9970	60	11273	11438	11684
Twin Ponds	414.5**	2	UCIAMS-121905	core 48	11070	40	12900	13000	13080
Blanding Lake	73	2	UCIAMS-190318	Charcoal	625	45	550	602	656
Blanding Lake	133	2	UCIAMS-190319	Charcoal	2225	35	2150	2226	2323
Blanding Lake	250	2	UCIAMS-190320	Charcoal	3450	70	3551	3709	3862
Blanding Lake	328	1	UCIAMS-190321	Charcoal	4280	20	4835	4847	4860
Blanding Lake	368	1	UCIAMS-190322	Charcoal	4410	20	4885	4977	5043
Blanding Lake	480*	2	UCIAMS-190323	Charcoal	16300	80	19526	19691	19861
Blanding Lake	541	1	UCIAMS-190324	Charcoal	7230	130	7833	8054	8294
Blanding Lake	577	1	UCIAMS-190325	Charcoal	7925	50	8621	8767	8967
Blanding Lake	652	2	UCIAMS-190326	Charcoal	8950	60	9900	10057	10208
Blanding Lake	738	1	UCIAMS-190327	Charcoal	12080	45	13821	13930	14052
Crooked Pond	62	1	UCIAMS-83271	Charcoal	1415	20	1297	1319	1344
Crooked Pond	77	1	UCIAMS-83272	Charcoal	2190	20	2130	2240	2298
Crooked Pond	100	1	UCIAMS-83273	Charcoal	2850	20	2886	2958	3039
Crooked Pond	110	1	UCIAMS-83274	Charcoal	3080	20	3235	3291	3354
Crooked Pond	128	1	UCIAMS-83275	Charcoal	3520	20	3723	3779	3858
Crooked Pond	139	1	UCIAMS-111581	Charcoal	4025	20	4428	4474	4531
Crooked Pond	142	1	UCIAMS-111582	Charcoal	4245	20	4733	4835	4849
Crooked Pond	152	1	UCIAMS-111583	Charcoal	4635	25	5317	5412	5447

Crooked Pond	176	1	UCIAMS-111584	Charcoal	4840	25	5488	5581	5596
Crooked Pond	181	1	UCIAMS-111585	Charcoal	4915	20	5597	5634	5691
Crooked Pond	205	1	UCIAMS-83276	Charcoal	4715	20	5333	5382	5554
Crooked Pond	350**	5	Beta- 94238	Bulk	6860	60	7605	7694	7817
Crooked Pond	624**	8	Beta- 94239	Bulk	9220	70	10258	10387	10549

Notes:
* Age reversal (not used in chronology)
** Twin Ponds: age from Core TP48 (Mandl et al., 2016); Crooked Pond age from Core D (Shuman et al., 2001)

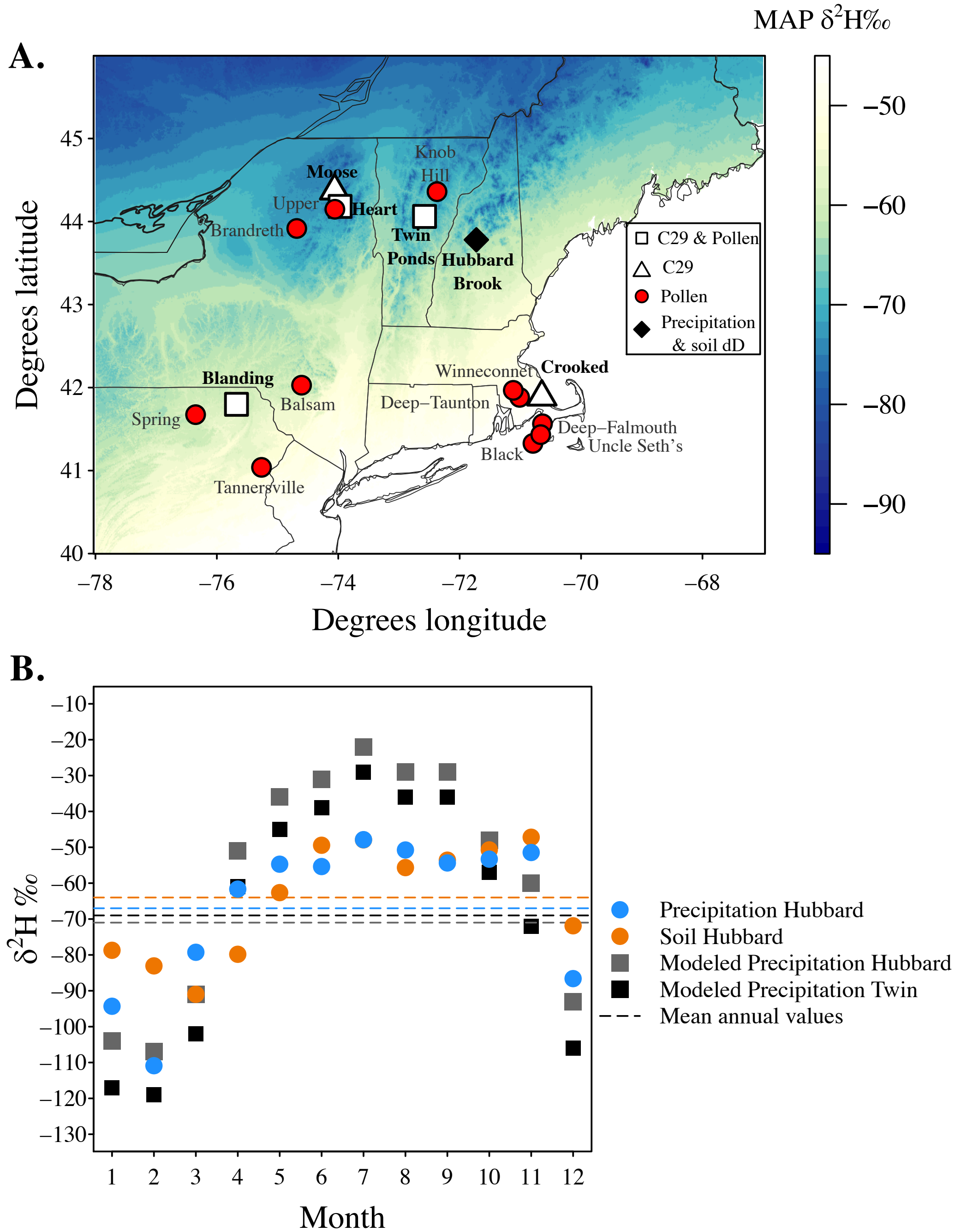

Figure 1. A. Map showing the northeastern U.S. region and the site locations for fossil pollen and *n*-C_{29}-alkane records; mean annual precipitation δ^2H values (δ^2H_{MAP}) are shown in the background with color scale to the right. **B.** Averaged monthly and annual δ^2H values of measured precipitation and soil moisture from Hubbard Brook (New Hampshire) and modeled monthly and annual precipitation δ^2H values at Hubbard Brook and Twin Ponds (Vermont).

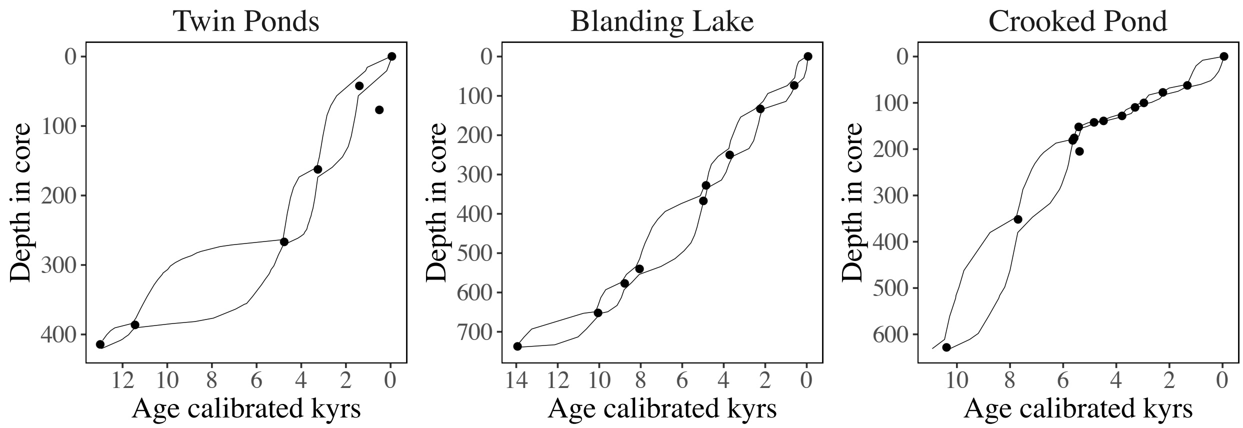

Figure 2. Age models for Twin Ponds (VT) (shallow water core), Blanding Lake (PA), and Crooked Pond (MA). Radiocarbon ages are shown with black circles and the black lines represent the 90^{th} percent credible intervals of modeled ages.

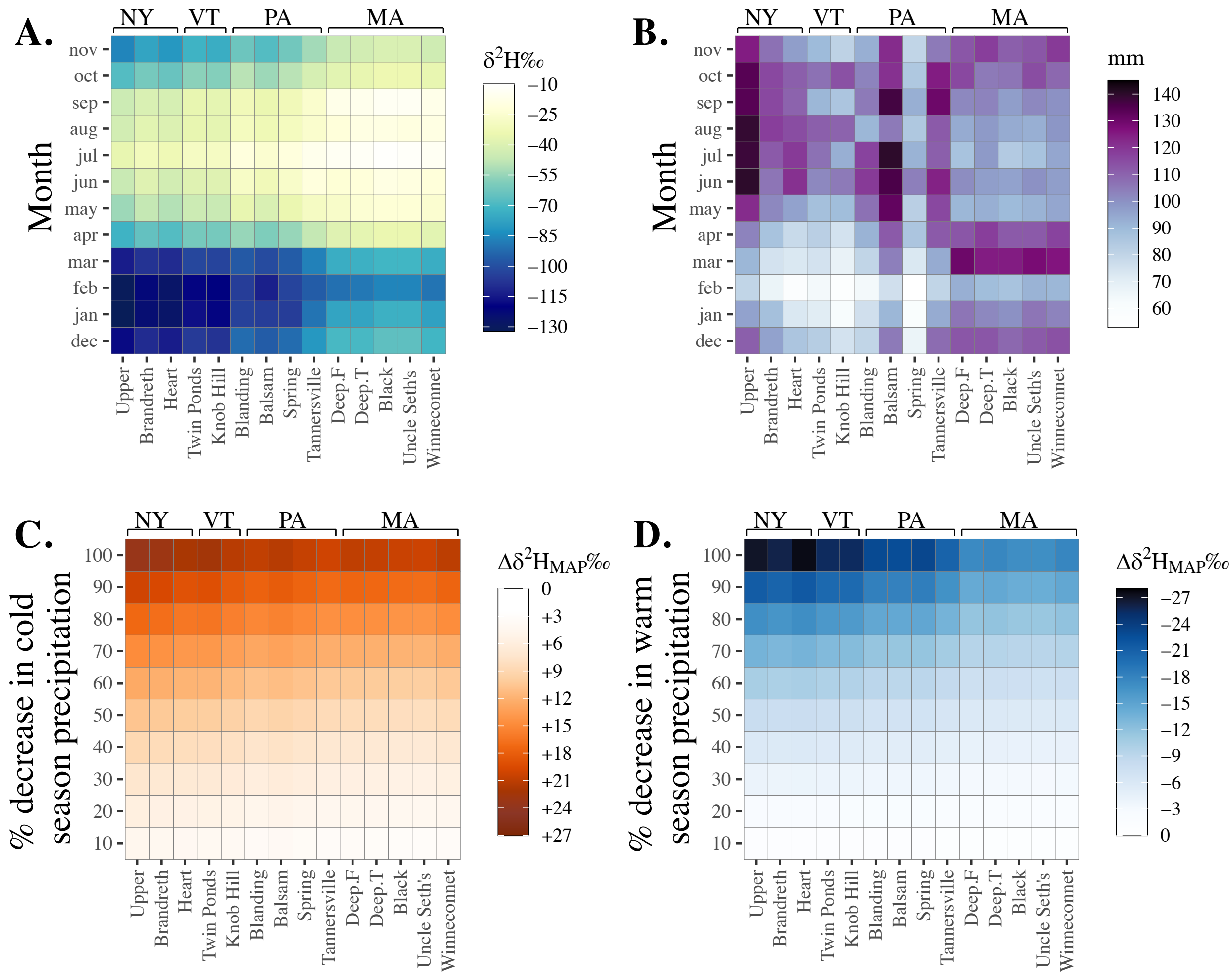

Figure 3. A. Monthly precipitation δ^2H values at individual sites (data from OIPC); **B.** Monthly precipitation input values at individual sites (data from Prism); **C.** Modeled change in δ^2H_{MAP} values as a function of % decrease in cold season precipitation at individual sites; **D.** Modeled change in δ^2H_{MAP} values as a function of % decrease in warm season precipitation at individual sites.

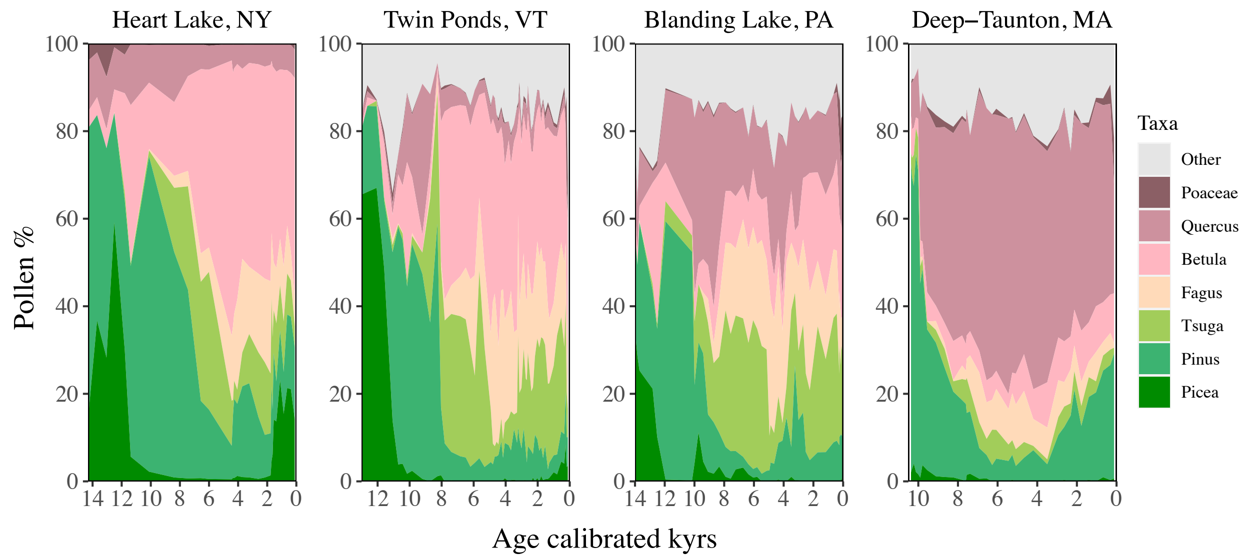

Figure 4. Changes in pollen percentages of major taxa vs. age at Heart Lake, Blanding Lake, Twin Ponds (deep-water core) and at the nearby Deep-Taunton Pond (closest to Crooked Pond, MA). Gymnosperm taxa are shown in green and angiosperm taxa are maroon. “Other” includes all other terrestrial pollen types from a list of 54 regional types used in the modern analog technique (Marsicek et al., 2013).

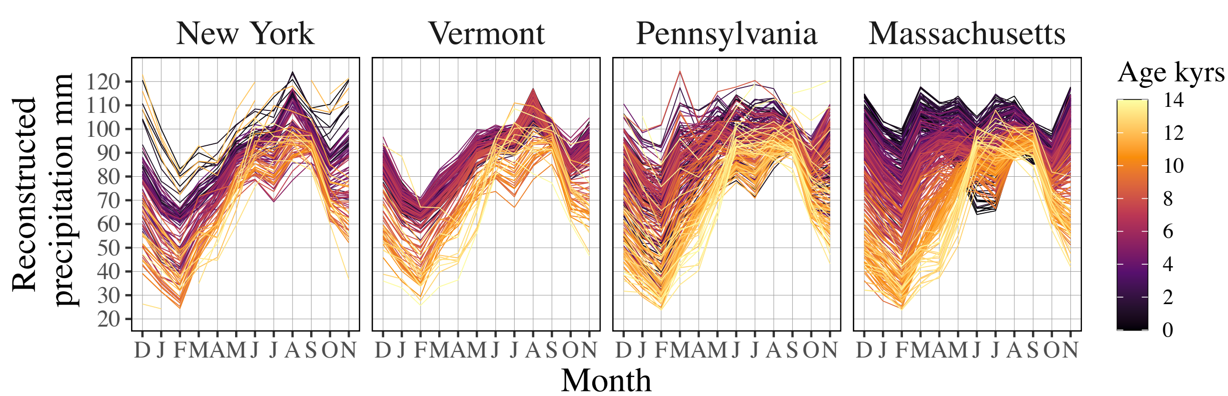

Figure 5. Pollen-inferred monthly precipitation values across individual regions (i.e., states) with calibrated age for color-scale. Each panel includes all the pollen-records from individual regions and black lines represent the monthly precipitation values for the core tops (i.e., modern).

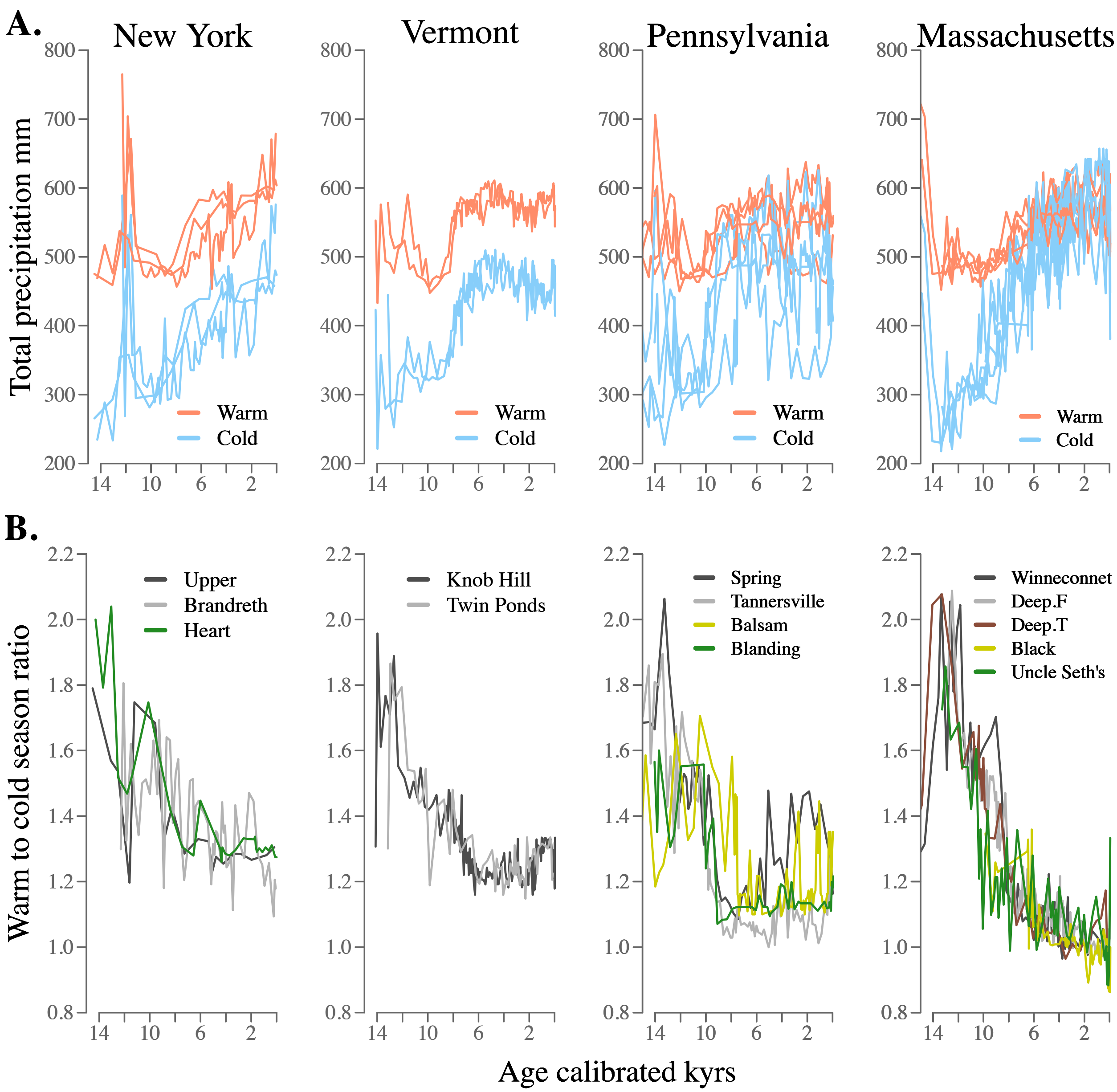

Figure 6. A. Pollen-inferred seasonal precipitation inputs: warm season shown in orange, cold season shown in blue. Each panel includes all the pollen records from individual regions. **B.** Warm to cold season ratio of precipitation plotted for individual pollen records as well as regionally.

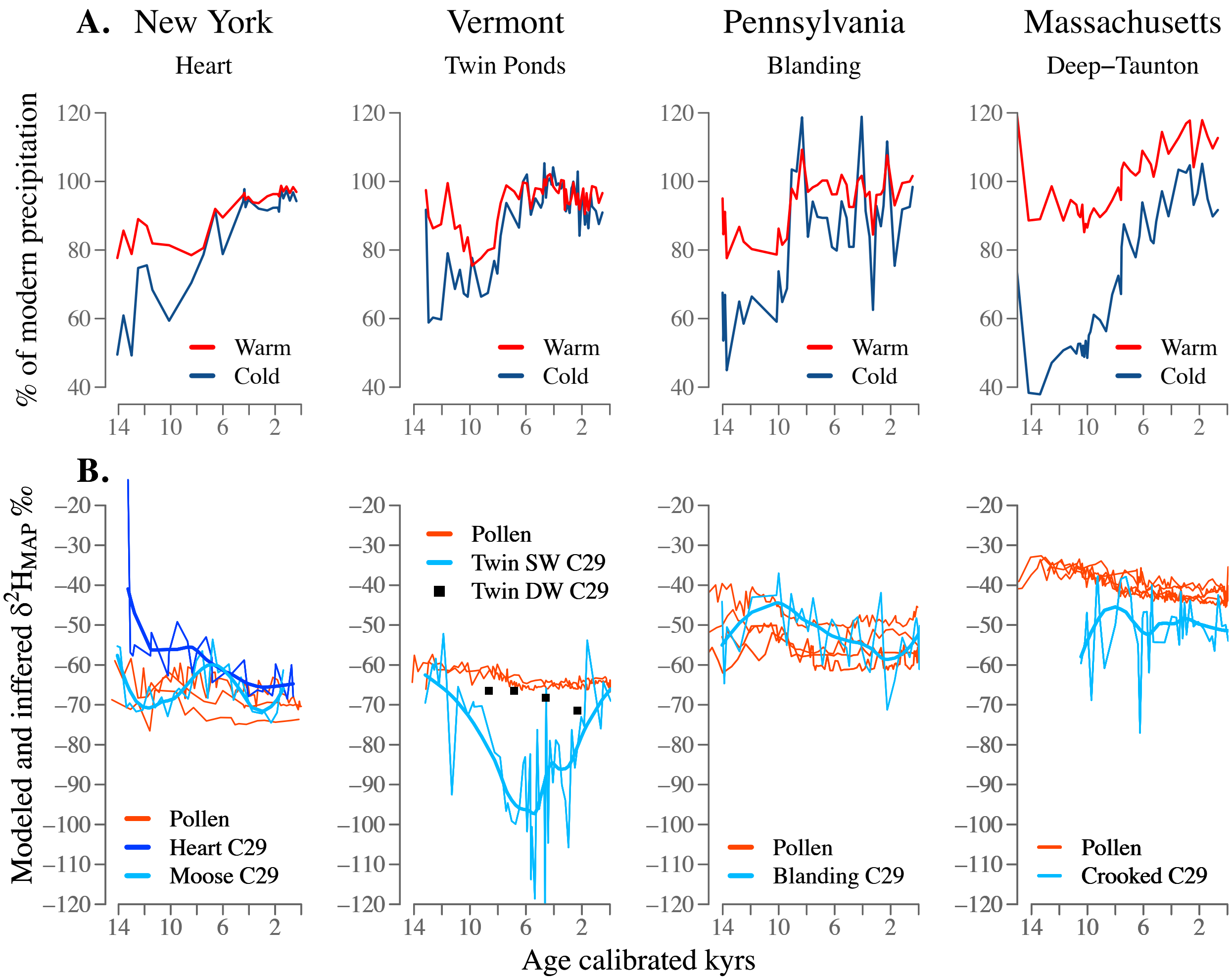

Figure 7. A. Pollen-inferred % of modern seasonal precipitation for selected sites; the last 600 years are excluded to avoid European land clearance effects on the reconstructions**. B.** Modeled δ^2H_{MAP} values at all fossil pollen sites based on pollen inferred seasonal changes in precipitation (orange lines) and reconstructed δ^2H_{MAP} values based on the *n*-C_{29}-alkane (blue lines). Reconstructed δ^2H_{MAP} values at Twin Ponds from the sediment core collected in the shallow, near-shore region of the lake (0.79 m depth) are shown in blue and labeled "Twin SW C29", while the reconstructed δ^2H_{MAP} values from the sediment core collected from the deepest location within the lake (7.8 m) are shown with black squares and labeled "Twin DW C29".